

Resurrecting light stops after the 125 GeV Higgs in the baryon number violating CMSSM

N. Chamoun,^{a,b} H. K. Dreiner,^b F. Staub^b and T. Stefaniak^b

^a*Physics Department, HIAST, P.O.Box 31983, Damascus, Syria*

^b*Bethe Center for Theoretical Physics and Physikalisches Institut, Universität Bonn, Bonn, Germany*

E-mail: nchamoun@th.physik.uni-bonn.de, dreiner@uni-bonn.de,
fnstaub@th.physik.uni-bonn.de, tim@th.physik.uni-bonn.de

ABSTRACT: In order to accommodate the observed Higgs boson mass in the CMSSM, the stops must either be very heavy or the mixing in the stop sector must be very large. Lower stop masses, possibly more accessible at the LHC, still give the correct Higgs mass only if the trilinear stop mixing parameter $|A_t|$ is in the multi-TeV range. Recently it has been shown that such large stop mixing leads to an unstable electroweak vacuum which spontaneously breaks charge or color. In this work we therefore go beyond the CMSSM and investigate the effects of including baryon number violating operators $\lambda'' \bar{U} \bar{D} \bar{D}$ on the stop and Higgs sectors. We find that for $\lambda'' \simeq \mathcal{O}(0.3)$ light stop masses as low as 220 GeV are consistent with the observed Higgs mass as well as flavour constraints while allowing for a stable vacuum. The light stop in this scenario is often the lightest supersymmetric particle. We furthermore discuss the importance of the one-loop corrections involving R -parity violating couplings for a valid prediction of the light stop masses.

KEYWORDS: Supersymmetry Phenomenology, Beyond the Standard Model

Contents

1	Introduction	1
2	The MSSM with Baryon Number Violation	2
3	Light stop, the Higgs mass and vacuum stability	4
3.1	Dominant (s)top corrections to the Higgs mass	4
3.2	Vacuum stability and R -parity violation	5
3.3	Loop corrections to the stop mass	7
4	Results	7
4.1	Numerical setup	7
4.2	Light stops in the CMSSM with $\bar{U}\bar{D}\bar{D}$ operators	10
5	Conclusion	14
A	Benchmark points	15
B	$\bar{U}\bar{D}\bar{D}$ corrections to stop masses	17
C	Minimising the scalar potential of the MSSM with $\bar{U}\bar{D}\bar{D}$ operators	19

1 Introduction

Run I of the the Large Hadron Collider (LHC) is complete. To date, there is no evidence for superpartner particles as predicted in supersymmetry (SUSY) [1] or experimental indications of any other physics beyond the Standard Model (SM).¹ The simplest SUSY scenarios like the constrained minimal supersymmetric standard model (CMSSM) [2] are under pressure by the ongoing non-discovery, leading to the exclusion of large areas of parameter space [3–6]. The observed Higgs boson mass of $m_h \approx 126$ GeV [7, 8] is within the previous predicted allowed range for supersymmetric models, including the CMSSM [9]. In order to have at least part of the SUSY spectrum moderately light and accessible at the LHC, *i.e.* stop masses of $m_{\tilde{t}_1} \lesssim 500$ GeV, it is necessary to maximise the mixing parameter in the stop sector, X_t [10]. However, it has been pointed out that large stop mixing in the (C)MSSM with rather light stop masses suffers from an unstable electroweak vacuum, such that charge or colour would be broken in a cosmologically short time [11–14]. A stable electroweak vacuum together with the correct Higgs mass implies a lower limit on the stop

¹See for example the talk given by O. Buchmüller at the EPS 2013 conference in Stockholm <https://indico.cern.ch/event/218030/session/28/contribution/869/material/slides/>.

mass of at least 800 GeV. At the same time the stop should not be too heavy, in order to avoid the fine-tuning related to the hierarchy problem, see for example Ref. [15].

These conclusions are restricted to the (C)MSSM. More recently, non-minimal SUSY models have gained more attention. For instance, singlet extensions which give additional tree-level contributions to the Higgs mass, soften significantly the little hierarchy problem of the MSSM and can accommodate a much smaller stop mixing while obtaining the correct Higgs mass [16–24]. However, there are also non-minimal SUSY models with the MSSM particle content with appealing properties. It has been pointed out that the MSSM together with R -parity violation (RpV) [25–28] can significantly weaken the collider mass limits [29–32] and provide a rich phenomenology [33–36]. It is the purpose of this paper to extend the (C)MSSM to allow for the R -parity baryon-number violating operators $\lambda''_{ijk} \bar{\mathbf{U}}_i \bar{\mathbf{D}}_j \bar{\mathbf{D}}_k$ and in this framework to determine the allowed stop mass regions, which give (a) the correct Higgs mass, (b) a charge and colour stable vacuum, and (c) fulfil all experimental constraints from flavour observables. We show that in this case it is possible to have light stop masses of a few hundred GeV together with a Higgs mass consistent with the LHC observations, but without introducing charge and colour breaking (CCB) minima.

The paper is organised as follows: in sec. 2 we introduce the model under consideration. In sec. 3 we explain the connection between the Higgs mass, light stops and the occurrence of charge and colour breaking minima in the baryon number violating CMSSM. In sec. 4 we present our numerical results, before we conclude in sec. 5. In the appendices we provide our benchmark points, sec. A, the one-loop RpV corrections to the squark masses, sec. B, as well as the minimum of the scalar potential, the vacuum, of the MSSM in the presence of $\lambda''_{ijk} \bar{\mathbf{U}}_i \bar{\mathbf{D}}_j \bar{\mathbf{D}}_k$ operators, sec. C.

2 The MSSM with Baryon Number Violation

R -parity is a discrete Z_2 symmetry of the MSSM which is defined as [25–28, 37]

$$R_P = (-1)^{3(B-L)+2s}, \quad (2.1)$$

where s is the spin of the field and B , L are its baryon respectively lepton number. We consider in the following the R -parity conserving superpotential of the MSSM

$$W_R = Y_e^{ij} \mathbf{L}_i \bar{\mathbf{E}}_j \mathbf{H}_d + Y_d^{ij} \mathbf{Q}_i \bar{\mathbf{D}}_j \mathbf{H}_d + Y_u^{ij} \mathbf{Q}_i \bar{\mathbf{U}}_j \mathbf{H}_u + \mu \mathbf{H}_u \mathbf{H}_d, \quad (2.2)$$

and extend it only by the renormalizable baryon number violating operators [38, 39]

$$W_{\not{B}} = \frac{1}{2} \lambda''_{ijk} \bar{\mathbf{U}}_i \bar{\mathbf{D}}_j \bar{\mathbf{D}}_k, \quad (2.3)$$

which also violate R -parity. Here $i, j, k = 1, 2, 3$ are generation indices, while we suppressed $SU(3)$ colour and $SU(2)$ isospin indices. In both of the previous equations \mathbf{L}_i , $\bar{\mathbf{E}}_j$, \mathbf{Q}_i , $\bar{\mathbf{U}}_i$, $\bar{\mathbf{D}}_i$, \mathbf{H}_d , \mathbf{H}_u denote the left chiral superfields of the MSSM in the standard notation [28]. We thus have for the total superpotential

$$W_{\text{tot}} = W_R + W_{\not{B}}. \quad (2.4)$$

This superpotential arises for example from the unique discrete gauge anomaly-free hexality Z_6^R . This is a discrete R-symmetry² and is derived and discussed in Ref. [42]. The low-energy μ term given in Eq. (2.2) is generated dynamically [43, 44].

For the superpotential in Eq. (2.4) the proton is stable, since lepton number is conserved, and the proton thus has no final state to decay to. However, heavier baryons can decay via double nucleon decay and virtual gluino or neutralino exchange [45], if λ'' couplings to light quarks are non-vanishing. However, we concentrate in the following exclusively on RpV couplings which involve the top quark. These are presently just bounded by perturbativity constraints [46], but could contribute at the one-loop level to flavour violating processes if the SUSY masses are not too heavy. For SUSY masses in the TeV range these effects are usually very small and do not provide better limits [47]. The main reason is that it is usually only possible to constrain products of λ'' couplings by flavour observables. However, we are going to consider in the following the case of only one non-vanishing λ'' at the GUT scale. Other couplings get induced via the RGE running because of the quark flavour violation but those remain small.

The corresponding standard soft supersymmetry breaking terms for the scalar fields $\tilde{L}, \tilde{E}, \tilde{Q}, \tilde{U}, \tilde{D}, H_d, H_u$ and the gauginos $\tilde{B}, \tilde{W}, \tilde{g}$ read

$$\begin{aligned} -\mathcal{L}_{\text{SB},R} = & m_{H_u}^2 |H_u|^2 + m_{H_d}^2 |H_d|^2 + \tilde{Q}^\dagger m_{\tilde{Q}}^2 \tilde{Q} + \tilde{L}^\dagger m_{\tilde{L}}^2 \tilde{L} + \tilde{D}^\dagger m_{\tilde{D}}^2 \tilde{D} + \tilde{U}^\dagger m_{\tilde{U}}^2 \tilde{U} + \tilde{E}^\dagger m_{\tilde{E}}^2 \tilde{E} \\ & + \frac{1}{2} \left(M_1 \tilde{B} \tilde{B} + M_2 \tilde{W}_a \tilde{W}^a + M_3 \tilde{g}_\alpha \tilde{g}^\alpha + h.c. \right) \\ & + (\tilde{Q} T_u \tilde{U}^\dagger H_u + \tilde{Q} T_d \tilde{D}^\dagger H_d + \tilde{L} T_e \tilde{E}^\dagger H_d + B_\mu H_u H_d + h.c.) \end{aligned} \quad (2.5)$$

$$-\mathcal{L}_B = \frac{1}{2} T''_{\lambda,ijk} \tilde{U}_i \tilde{D}_j \tilde{D}_k + h.c.. \quad (2.6)$$

Here we have suppressed all generation indices, except in the last RpV term. The $m_{\tilde{F}}^2$ are 3×3 matrices and denote the squared soft masses of the scalar components \tilde{F} of the corresponding chiral superfields F . The $T_{u,d,e}$ are 3×3 matrices of mass-dimension one. They are trilinear coupling constants of the scalar fields, and can be written in terms of the standard A -terms [48] if no flavour violation is assumed, $T_{ii}^f = A_i^f Y_f^{ii}$, with $i = 1, 2, 3$, and no summation over repeated indices, and $f = e, u, d$. Similarly, for the baryon number violating term we have $T''_{\lambda,ijk} = A''_{ijk} \lambda''_{ijk}$, again with no summation.

Already the general, R -parity conserving MSSM with massless neutrinos has 105 parameters beyond those of the SM [49]. In the R -parity violating sector, as shown, there are 36 additional parameters. Note that λ''_{ijk} and $T''_{\lambda,ijk}$ are anti-symmetric in the last two indices and can be complex. In order to significantly reduce the number of free parameters, we study a constrained model similar to the R -parity conserving CMSSM. As usual, we demand that all soft-breaking masses are universal at the grand unification (GUT) scale, $M_{\text{GUT}} = \mathcal{O}(10^{16} \text{ GeV})$. In addition, we treat the soft-breaking RpV couplings $T''_{\lambda,ijk}$ in the same way as the trilinear soft-breaking couplings of the MSSM, *i.e.* we assume that it is proportional to the corresponding superpotential term at M_{GUT} , with a universal

²For a discussion of R-symmetries see for example Refs. [40, 41].

proportionality constant A_0 . Thus, our boundary conditions at M_{GUT} are

$$m_0^2 \equiv m_{H_d}^2 = m_{H_u}^2, \quad 1m_0^2 \equiv m_{\tilde{Q}}^2 = m_{\tilde{D}}^2 = m_{\tilde{U}}^2 = m_{\tilde{E}}^2 = m_{\tilde{L}}^2 \quad (2.7)$$

$$M_{1/2} \equiv M_1 = M_2 = M_3 \quad (2.8)$$

$$T_\lambda'' \equiv A_0 \lambda'', \quad T_i \equiv A_0 Y_i \quad \text{with } i = e, d, u. \quad (2.9)$$

The parameters μ and B_μ are fixed by the minimisation conditions of the vacuum ground state and we always set $\mu > 0$. We furthermore assume that all CP-violating phases vanish.

3 Light stop, the Higgs mass and vacuum stability

3.1 Dominant (s)top corrections to the Higgs mass

The main corrections to the light Higgs mass in the MSSM at one-loop stem from the (s)top contributions. They can be written in the decoupling limit $M_A \gg M_Z$ as [1, 9, 10, 50–52]

$$\delta m_h^2 = \frac{3}{2\pi^2} \frac{m_t^4}{v^2} \left[\log \frac{M_S^2}{m_t^2} + \frac{X_t^2}{M_S^2} \left(1 - \frac{X_t^2}{12M_S^2} \right) \right] \quad (3.1)$$

with $M_S \equiv \sqrt{m_{\tilde{t}_1} m_{\tilde{t}_2}}$, m_t being the running $\overline{\text{DR}}$ top mass and $X_t \equiv A_t - \mu \cot \beta$. Our convention for the electroweak vacuum expectation value (vev) is $v \simeq 246$ GeV. If one wants to keep $m_{\tilde{t}_i}$ moderately low (around or even below 1 TeV) the loop corrections required to explain the measured Higgs mass can be achieved by maximising the contributions proportional to the stop mixing X_t . δm_h^2 becomes maximal for $X_t = \sqrt{6}M_S$. In the following, we want to discuss the dependence of the light Higgs mass on X_t and $m_{\tilde{t}_1}$ in more detail. For this purpose we show in Fig. 1 the approximate values of the light Higgs mass at the one-loop level as function of these two parameters, respectively, keeping the other two fixed. The plots are based on the approximate formula given in Eq. (3.1). One can see that the light stop mass can be reduced by a few hundred GeV, for fixed values of X_t , without affecting the one-loop corrections to the light Higgs mass substantially. However, it is *not* possible in the CMSSM to change $m_{\tilde{t}_1}$ without affecting X_t and/or $m_{\tilde{t}_2}$, because all three parameters depend on m_0 , A_0 and $\tan \beta$. This is problematic because it has recently been pointed out that the maximal mixing scenario, $X_t = \sqrt{6}M_S$, in the context of a light SUSY spectrum is ruled out by the instability of the electroweak (EW) vacuum: The required large values of $|A_0|$ compared to m_0 lead to minima in the scalar potential below the EW vacuum, where colour and charge are broken by vacuum expectation values of stops or staus [11–13]. Furthermore, the EW vacuum would decay in a cosmologically short time. The condition of a stable EW vacuum can be used to put a lower limit on the light stop mass in the R -parity conserving CMSSM: one can determine the maximal value of $|A_0|$ allowed by vacuum stability for fixed values of $\{m_0, M_{1/2}, \tan \beta\}$. This value can be translated into the minimal allowed stop mass for a given combination of $\{m_0, M_{1/2}, \tan \beta\}$. These limits have been derived in Ref. [11] and we present examples in Fig. 2. For $m_0 > 1$ TeV, $M_{1/2} > 1$ TeV it is not possible to get a light stop mass below 1 TeV. Lighter stops are possible for smaller values of $M_{1/2}$. However, this is often in conflict with current lower limits from gluino searches [53]. The constraint from the Higgs mass measurement has not yet been applied at this point.

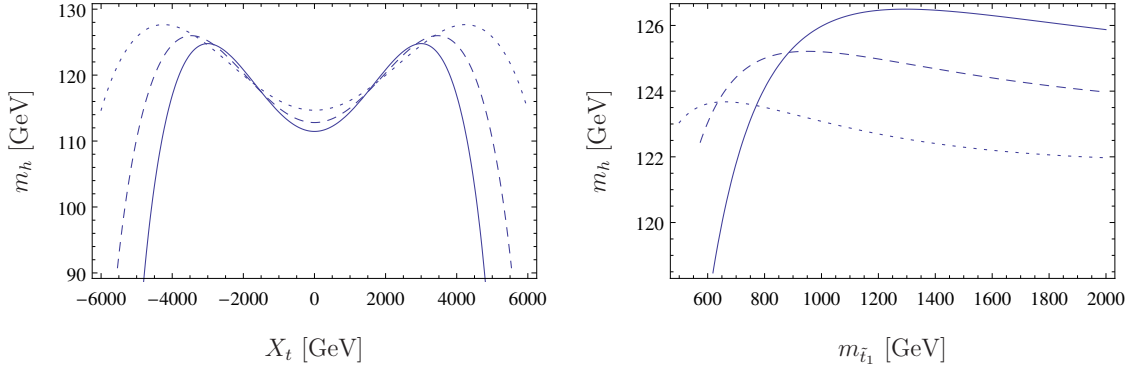


Figure 1. On the left: approximation of the light Higgs mass at one-loop as a function of X_t with $m_{\tilde{t}_1} = 750$ GeV (dotted), $m_{\tilde{t}_1} = 1000$ GeV (dashed), $m_{\tilde{t}_1} = 1500$ GeV (full). On the right: m_h as a function of $m_{\tilde{t}_1}$ with $X_t = -2.5$ TeV (dotted), $X_t = -3$ TeV (dashed), $X_t = -3.5$ TeV (full). In both plots we set $m_{\tilde{t}_2} = 2$ TeV.

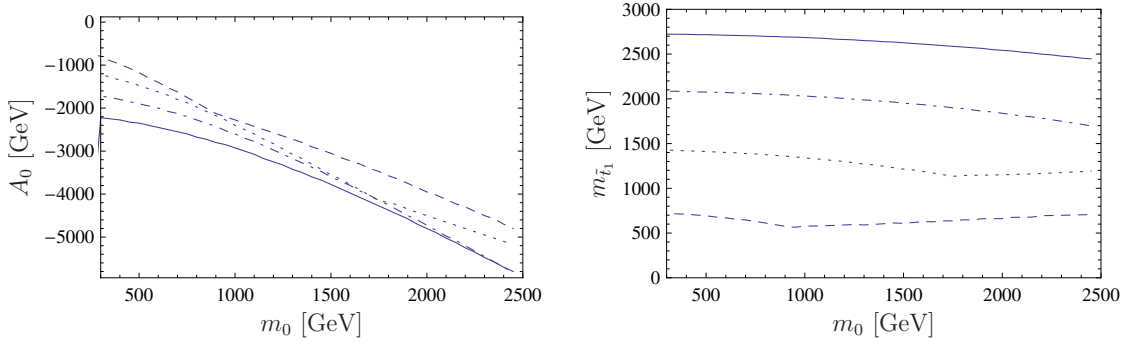


Figure 2. Left: the minimal value of A_0 in GeV compatible with a stable EW vacuum as a function of m_0 for $M_{1/2} = 0.5$ TeV (dashed), 1.0 TeV (dotted), 1.5 TeV (dot-dashed), 2.0 TeV (full) and $\tan\beta = 15$. Right: for the corresponding value of $A_0(m_0)$ of a given point in the left figure we compute the lightest stop mass. This is shown on the right as a function of m_0 for the same choices of $M_{1/2}$. We set $\tan\beta = 15$ in all cases.

3.2 Vacuum stability and R -parity violation

The situation described above changes if one allows for non-vanishing R -parity violating couplings. These affect at one-loop for example the running of $T_{u,33} = A_t Y_u^{tt}$ and $m_{u,33}^2 = m_{\tilde{t}_R}^2$ [28]:

$$\beta_{T_{u,ij}}^{(1)} = \beta_{T_{u,ij}}^{(1),\text{MSSM}} + 2\lambda_{abc}'' Y_{u,aj} T_{\lambda_{ibc}}'' + \lambda_{cab}'' \lambda_{iab}'' T_{u,cj}, \quad (3.2)$$

$$\begin{aligned} \beta_{m_{\tilde{U},ij}^2}^{(1)} = & \beta_{m_{\tilde{U},ij}^2}^{(1),\text{MSSM}} + 2T_{\lambda_{jab}}'' T_{\lambda_{iab}}'' \\ & + 4\lambda_{jac}'' \lambda_{iab}'' m_{\tilde{D},cb}^2 + \lambda_{cab}'' \lambda_{iab}'' m_{\tilde{U},cj}^2 + \lambda_{jbc}'' \lambda_{abc}'' m_{\tilde{U},ia}^2. \end{aligned} \quad (3.3)$$

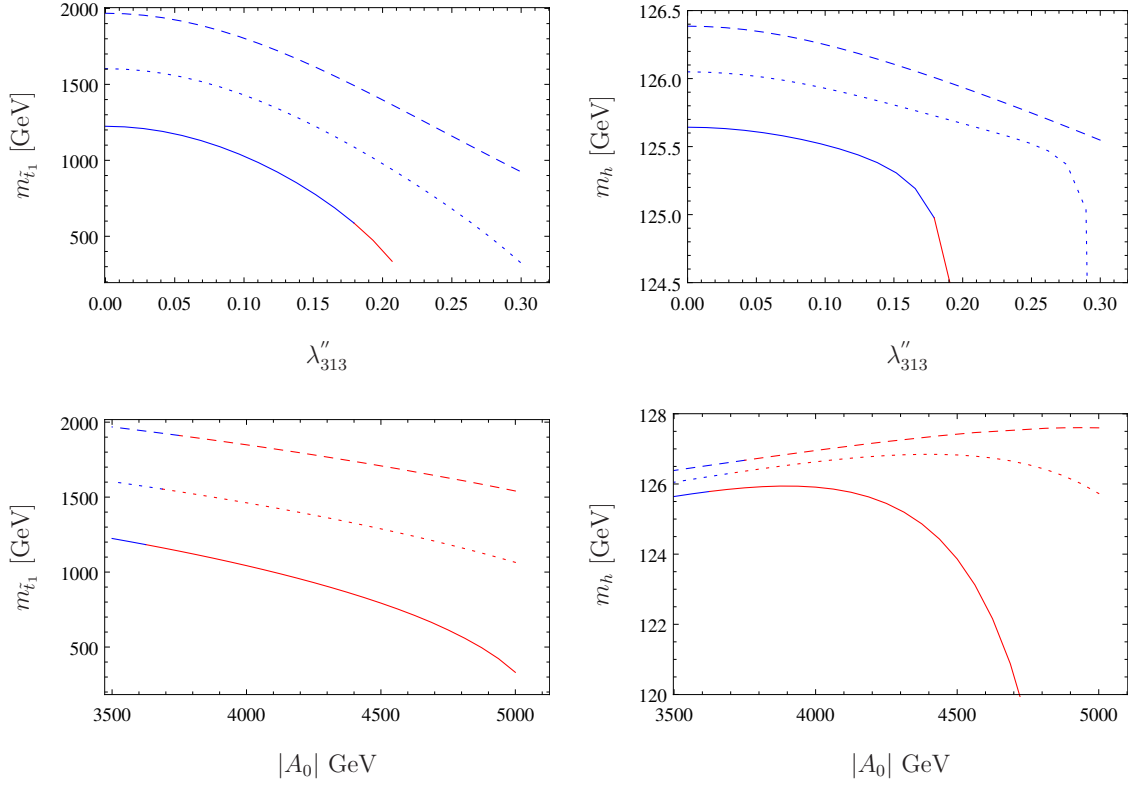


Figure 3. First row: the lightest stop mass, $m_{\tilde{t}_1}$, (left) and light Higgs mass, m_h , (right) as a function of the R -parity violating coupling λ''_{313} evaluated at M_{GUT} . Here, we set $m_0 = 1500$ GeV, $\tan \beta = 12$, $A_0 = -3500$ GeV and $\mu > 0$. The solid lines are for $M_{1/2} = 1000$ GeV, the dotted lines are for $M_{1/2} = 1250$ GeV, and the dashed lines are for $M_{1/2} = 1500$ GeV. Second row: Dependence of $m_{\tilde{t}_1}$ (left) and m_h (right) on A_0 (we consider only $A_0 < 0$ here) in the R -parity conserving case, $\lambda''_{313} = 0$. The remaining parameters are chosen as in the first row. The blue lines correspond to a stable and the red lines to a meta-stable EW vacuum.

To demonstrate the consequences of these additional terms, we show as an example the affect of $\lambda''_{313}(M_{\text{GUT}})$ on the weak scale values of $m_{\tilde{t}_1}$ and m_h in Fig. 3. We already distinguish here between points with a stable and an unstable EW vacuum. For these plots we have used our full numerical setup, explained in detail below in sec. 4.1.

Here, we start with a fixed set of CMSSM parameters $\{m_0, M_{1/2}, \tan \beta, A_0\}$ with a stable EW vacuum and then turn on λ''_{313} . We see that the light stop mass can be reduced by several hundred GeV without spoiling the vacuum stability or affecting the light Higgs mass too much. For comparison, we show also the impact of a variation of A_0 while keeping $\lambda''_{313} = 0$. This reduces also the light stop mass as expected and has a much larger impact on the Higgs mass. However, values of A_0 below -3.7 TeV are forbidden because the vacua where charge and colour are broken become deeper than the EW vacuum. Thus, baryon number violating couplings are a very attractive possibility to obtain light stop scenarios in the CMSSM which are not in conflict with vacuum stability.

3.3 Loop corrections to the stop mass

We have seen that light stops and the correct Higgs mass can be obtained for large values of λ''_{31i} if the operator couples directly to the top quark. However, the R -parity violating coupling will not only change the RGE running, as discussed in Ref. [28, 54], but also contribute to the radiative corrections to the stop masses at the one-loop level. Since these corrections to the stop masses to our knowledge have not been considered so far in the literature, we discuss the effect here. The analytical calculation is summarised in Appendix B. We find that the corrections to the right-stop mass squared are approximately given by

$$\delta m_{\tilde{t}_R}^2 \simeq \frac{1}{8\pi^2} |\lambda''_{3ij}|^2 M_{SUSY}^2. \quad (3.4)$$

Here, M_{SUSY} is taken to be the mass scale of the down-like squarks running in the loop. If these masses are much heavier than the stop they can give large positive contributions to the light stop mass.

To show the importance of these corrections we present in Fig. 4 the mass of the light stop as function of λ''_{313} and m_0 at tree and one-loop level. We present in the top figures λ''_{313} evaluated at both M_{GUT} and M_{SUSY} . At one-loop we give the results with and without the R -parity violating corrections to the stop self-energies. These results are based on a full numerical calculation which does not rely on the simplifying assumptions made in Appendix B. All effects of flavour mixing, mass difference between squarks, and of the external momentum are taken into account. The numerical calculation is based on the general procedure to calculate one-loop mass spectra with the **Mathematica** package **SARAH**, presented in Ref. [55, 56].

We can see that for light stops the loop corrections are very important. They are dominated by the α_s corrections if the $\bar{U}\bar{D}\bar{D}$ contributions are neglected. These corrections are negative and quickly reduce the tree-level mass in the limit $m_{\tilde{g}} \gg m_{\tilde{t}_1}$ [57]. In contrast, the $\bar{U}\bar{D}\bar{D}$ corrections are positive and stabilise the stop mass at the one-loop level. We see that these corrections can easily shift the stop mass by more than 100 GeV compared to the case of an R -parity conserving one-loop calculation. Thus, these corrections have to be taken into account for any meaningful prediction of light stop masses in the context of large R -parity violating couplings.

4 Results

We are interested in parameter regions in the CMSSM extended by baryon number violating operators, which provide a light stop. As constraints, we take the Higgs mass measurement, the limits on new physics from flavour observables and the stability of the EW vacuum. Before we present the preferred regions, we give the main details of our numerical setup.

4.1 Numerical setup

We have used **SARAH** [55, 58–61] to obtain a **SPheno** [62, 63] version of the MSSM with trilinear RpV . This **SPheno** version calculates the renormalisation group equations (RGEs) taking into account the full RpV effects at the one- and two-loop level. The RGEs have

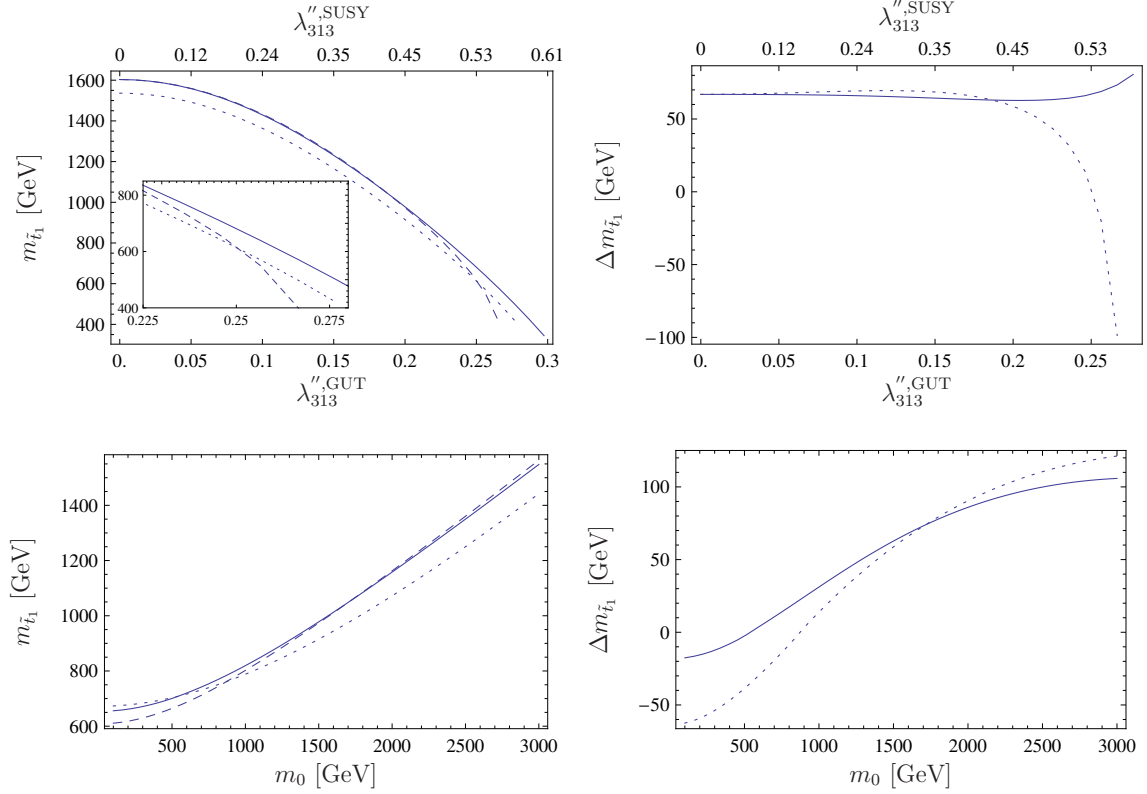


Figure 4. First row: the lightest stop mass, $m_{\tilde{t}_1}$, as a function of the R -parity violating coupling λ''_{313} , evaluated either at M_{GUT} (bottom axis labels) or at M_{SUSY} (top axis labels). We set $m_0 = 1500$ GeV, $M_{1/2} = 1250$ GeV, $\tan\beta = 12$, $A_0 = -3500$ GeV, and $\mu > 0$. On the left we show the tree-level mass (dotted line), the one-loop mass without $\bar{U}\bar{D}\bar{D}$ corrections (dashed line) and the mass with full one-loop corrections (full line). On the right we show the mass difference between the tree-level and the one-loop mass ($\Delta m_{\tilde{t}_1} = m_{\tilde{t}_1}^{(1L)} - m_{\tilde{t}_1}^{(T)}$) with (full line) and without (dotted line) $\bar{U}\bar{D}\bar{D}$ corrections. Note that the contributions of the $\bar{U}\bar{D}\bar{D}$ operators to the RGE running are included in all cases. Second row: $m_{\tilde{t}_1}$ as function of m_0 . Here we fixed $\lambda''_{313}^{\text{GUT}} = 0.2$. The other parameters are chosen as in the first row.

been cross checked against Refs. [28, 54]. In addition, the program calculates the entire mass spectrum at the one-loop level. Thus, also the one-loop corrections to the stop masses stemming from λ''_{31i} discussed in sec. 3.3 are included. Furthermore, the known two-loop corrections to the light Higgs mass are taken into account [64–67]. We have compared the mass spectrum calculation of this **SPheno** version with **SoftSusy** 3.3.8 [68, 69]. We found good agreement if we remove the radiative R pV corrections to the mass spectrum, which are not included in **SoftSusy**. The remaining differences are of the same size as the known discrepancies in the MSSM [70] and provide an estimate of the theoretical uncertainty.

Moreover, **SPheno** calculates the decay widths and branching ratios of the Higgs boson(s), as well as the Higgs couplings normalised to the SM expectations. We employ this information through **HiggsBounds** [71–74] and **HiggsSignals** [75, 76] to confront the Higgs

sector for a given parameter point with existing measurements and exclusion limits. This has almost no influence on our results, as the stops we obtain are too heavy [77].

There are also a wide range of flavour observables calculated by **SPheno** with a high precision even for SUSY models beyond the MSSM, thanks to the **FlavorKit** interface [78], which is an automatisisation of the approach presented in Ref. [79]. We consider in the following the observables $B \rightarrow X_s \gamma$, $B_q^0 \rightarrow \mu^+ \mu^-$, and ΔM_{B_q} ($q = s, d$), which provide the best limits. To accept or discard parameter points based on the flavour observables we consider the ratio $R(X)$ defined as

$$R(X) \equiv \frac{X}{X_{SM}}. \quad (4.1)$$

Here X is the predicted value of each flavour observable for a given parameter point, and X_{SM} is the corresponding SM theoretical expectation. If we assume a 10% uncertainty in the SUSY calculation and combining the experimental limits together with the corresponding SM predictions, we get the following constraints at 95% C.L. on the $R(X)$:

- $B \rightarrow X_s \gamma$ [80–84]

$$0.89 < R(\text{BR}(b \rightarrow s \gamma)) < 1.33 \quad (4.2)$$

- $B_q \rightarrow l^+ l^-$ [47, 84–86]

$$0.43 < R(\text{BR}(B_s \rightarrow \mu^+ \mu^-)) < 1.35 \quad (4.3)$$

$$R(\text{BR}(B_d \rightarrow \mu^+ \mu^-)) < 8.3 \quad (4.4)$$

- ΔM_{B_q} [83, 87–89]

$$0.54 < R(\Delta M_{B_s}) < 1.44 \quad (4.5)$$

$$0.25 < R(\Delta M_{B_d}) < 1.84 \quad (4.6)$$

To check the vacuum stability of each parameter point we use the computer program **Vevacious** [90], for which we have created the corresponding model files with **SARAH**. For this step, we had to restrict ourselves to a set of particles, which can in principle get a non-vanishing vev. Since the required computational effort grows quickly with the number of allowed vevs, we employ a two step approach: First, we assume that only the staus and stops can have non-vanishing vevs ($v_{\tau_L}, v_{\tau_R}, v_{t_L}, v_{t_R}$), besides those for the neutral Higgs scalar fields. All points which pass this check, *i.e.* they do not have a charge or colour breaking minimum, are again checked for the global vacuum taking into account the vevs of those generations of down-squarks which are involved in the λ''_{3ij} coupling ($v_{t_L}, v_{t_R}, v_{D_L^i}, v_{D_R^i}, v_{D_L^j}, v_{D_R^j}$). Here it is necessary to allow also for vevs of the left-handed counterparts of the right down-like squarks to find D -flat directions in the scalar potential, even though they do not couple directly to $\bar{\mathbf{U}}\mathbf{D}\mathbf{\bar{D}}$. The scalar potential at tree-level is discussed in more detail in Appendix C. As discussed there, the additional checks for CCB vacua with down-like squark vevs should have only a minor impact on the number of points which are ruled out by the vacuum considerations. This is confirmed by our numerical study: only

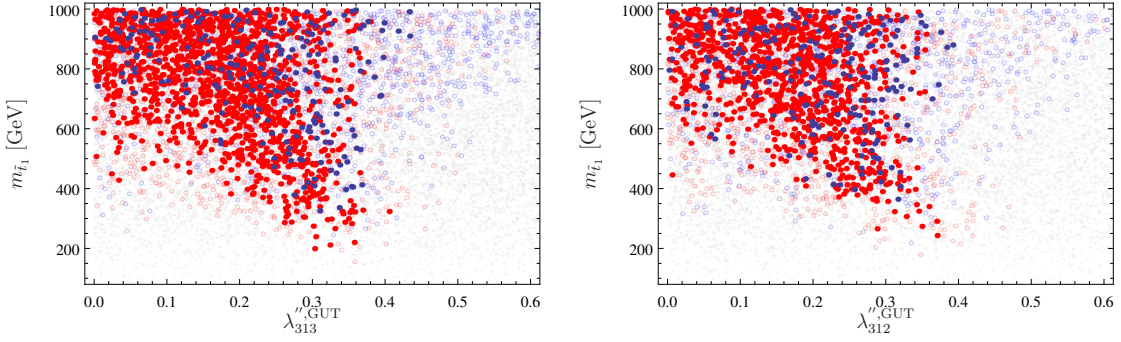


Figure 5. Vacuum stability in the $(\lambda_{313}^{\prime\prime, \text{GUT}}, m_{\tilde{t}_1})$ (left) and $(\lambda_{312}^{\prime\prime, \text{GUT}}, m_{\tilde{t}_1})$ (right) planes based on a random scan using the parameter ranges of Eqs. (4.7) and (4.8). The blue points have a stable EW vacuum while for the red points deeper CCB vacua exist. For the filled dots we required $m_h \in [124, 128]$ GeV, and for the large empty circles we applied $m_h \in [122, 130]$ GeV as a cut. The small empty grey circles are without any cut on the Higgs mass but have a stable vacuum.

5% of the points with stop masses below 1 TeV, which seem to be stable when checking only for stau and stop vevs, are in fact only meta-stable when including the sdown and sbottom vevs in addition ($\lambda_{313}^{\prime\prime}$ -case). For $\lambda_{312}^{\prime\prime}$ no points are affected by the additional check for vacua with sdown and sstrange vevs.

In the following, we only accept points which do not exhibit a deeper CCB vacuum. In principle, it might be possible that the EW vacuum is only meta-stable, but long-lived on a cosmological time scale. However, it is been shown that vacua which seem to be long-lived at zero temperature are likely to have tunnelled in the early universe into the CCB vacuum if temperature effects are taken into account [14].

4.2 Light stops in the CMSSM with $\bar{U}\bar{D}\bar{D}$ operators

To find regions with light stops in the CMSSM in the presence of $\bar{U}\bar{D}\bar{D}$ operators in agreement with all constraints, we performed random scans with the tool SSP [91] restricted to the following ranges of CMSSM parameters

$$m_0 \in [0, 2] \text{ TeV}, \quad M_{1/2} \in [0, 2] \text{ TeV}, \quad \tan \beta \in [5, 60], \quad A_0 \in [-10, 0] \text{ TeV}, \quad \mu > 0. \quad (4.7)$$

For the $\bar{U}\bar{D}\bar{D}$ parameters we have chosen the range

$$\lambda_{31i}^{\prime\prime} \in [0, 0.7] \quad \text{with } i = 2, 3, \quad (4.8)$$

as the input at the GUT scale. The results are summarised in Fig. 5. Here, we have applied two different cuts on the Higgs mass: $m_h = (126 \pm 4)$ GeV or the stricter case $m_h = (126 \pm 2)$ GeV. The second cut is motivated by the theoretical uncertainty for the light Higgs mass of 2–3 GeV, which is usually assumed when using the known two-loop results. However, the $\lambda_{3ij}^{\prime\prime}$ couplings give rise to new corrections to the Higgs mass at two-loop. These contributions are unknown and increase therefore the theoretical uncertainty.

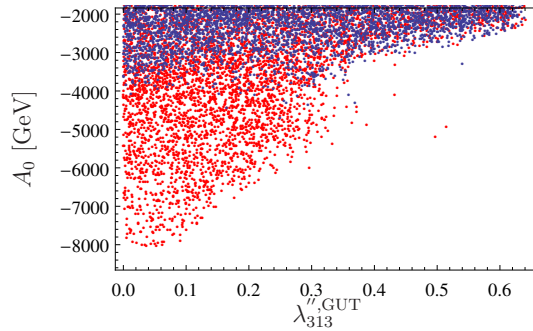


Figure 6. Allowed values for A_0 as function of $\lambda_{313}^{''GUT}$. The blue points have a stable EW vacuum while for the red points deeper CCB vacua exist. No cut is imposed on the light Higgs mass.

In Fig. 5, the blue points have a stable EW vacuum while for the red points deeper CCB vacua exist. For the filled dots we required $m_h \in [124, 128]$ GeV, while for the large empty (red and blue) circles we applied the weaker constraint $m_h \in [122, 130]$ GeV. The small empty grey circles are without any cut on the Higgs mass, but have a stable vacuum. The figure on the left differs from that on the right slightly, due to the lighter sbottom mass to be applied in Eq. (3.4). The corresponding plot for $\lambda_{323}^{''}$ is indistinguishable from that presented here for $\lambda_{313}^{''}$.

We can see the general trend: For increasing $\lambda_{31i}^{''}$ a lighter and lighter stop mass is compatible with all constraints. One central result of this paper is that we can have a stop mass as low as 220 GeV while satisfying the strict Higgs mass constraint and also having a stable EW vacuum, for $\lambda_{31j}^{''} \gtrsim 0.3$.

We see that the Higgs mass limit has a large impact on the preferred regions in the $(\lambda_{31i}^{''}, m_{\tilde{t}_1})$ plane: if no cut on the light Higgs mass is applied, the full planes shown in Fig. 5 are populated with (small empty grey) circles which have a stable EW vacuum. However, using $m_h \in [122, 130]$ GeV makes it much more difficult to find viable points with $\lambda_{31i}^{''} > 0.4$, and stop masses below 1 TeV. This can be understood from Fig. 6, where we show the correlation between A_0 and $\lambda_{313}^{''}$: If $\lambda_{313}^{''}$ increases, the upper limit of $|A_0|$ allowed by a non-tachyonic spectrum decreases. For $\lambda_{313}^{''} > 0.4$ a spectrum without tachyons requires $A_0 > -3000$ GeV. For larger values of $|A_0|$, the $T_\lambda^{''}$ contributions to the running of m_U^2 shown in Eq. (3.3) cause a negative soft SUSY breaking mass squared term for the right-handed stop. However, these values of $|A_0|$ are not sufficient to lift the light Higgs mass above the lower limit of 122 GeV, if the stop is too light. As a consequence, the maximal value for the light Higgs mass that we find decreases with increasing $\lambda_{31i}^{''}$, because of the simultaneously decreasing stop mass. This behaviour can also be seen in Fig. 7.

For small or vanishing $\lambda_{31i}^{''}$ couplings and a Higgs mass above 124 GeV the minimal stop mass with a stable EW vacuum is above 800 GeV. This is in agreement with our expectations based on Fig. 2. In contrast, we find for $\lambda_{313}^{''} \sim 0.3$ points with stop masses below 400 GeV which do not suffer from a deeper CCB vacuum.

If we relax the bound on the heavy Higgs mass and use as the lower limit 122 GeV,

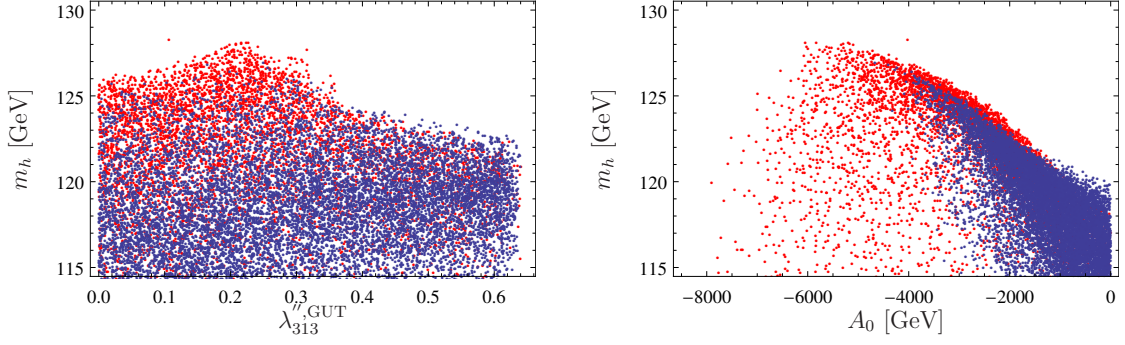


Figure 7. Dependence of the light Higgs mass m_h on $\lambda_{313}^{''\text{GUT}}$ (left) and A_0 (right). All points fulfil $m_{\tilde{t}_1} < 1$ TeV. The blue points have a stable EW vacuum while for the red points deeper CCB vacua exist. In the scan, no constraint has been imposed on the Higgs mass here. We do require $m_{\tilde{t}_1} < 1$ TeV

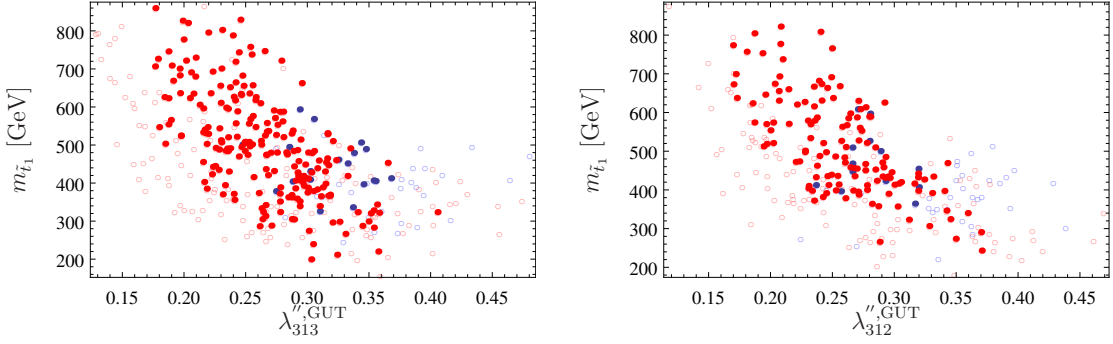


Figure 8. Vacuum stability in the $(\lambda_{313}^{''\text{GUT}}, m_{\tilde{t}_1})$ plane (on the left) and $(\lambda_{312}^{''\text{GUT}}, m_{\tilde{t}_1})$ plane (on the right) showing only points with a stop lightest supersymmetric particle (LSP). The blue points have a stable EW vacuum while for the red points deeper CCB vacua exist. For the filled dots we required $m_h \in [124, 128]$ GeV, while for the empty circles we only required $m_h \in [122, 130]$ GeV.

we find in the R -parity conserving limit ($\lambda_{31i}^{''} \ll 0.1$) already points with stop masses below 350 GeV. However, for these small $\lambda_{31i}^{''}$ couplings a theoretical uncertainty of 4 GeV on the light Higgs mass might be overestimated. In addition, these points usually have a small value of $M_{1/2}$, as seen in Fig. 2. This implies a light gluino mass which would be in conflict with current mass limits [92], for $\lambda_{31i}^{''} = 0$. Furthermore, in the case of non-zero $\lambda_{31i}^{''}$, constraints from LHC searches for three-jet resonances from gluinos apply [93, 94]. Thus it is questionable if these points should be considered at all. Nevertheless, also for this very conservative limit on the Higgs mass, one can find parameter points with even lighter stops if sizeable R pV couplings are present. In general, we find in our scans that $\lambda_{313}^{''} \simeq 0.3$ turns out to be the optimal value to find parameter points with a light stop with $m_{\tilde{t}_1} \sim (220 - 250)$ GeV, a Higgs mass in agreement with the measurement and a stable EW vacuum.

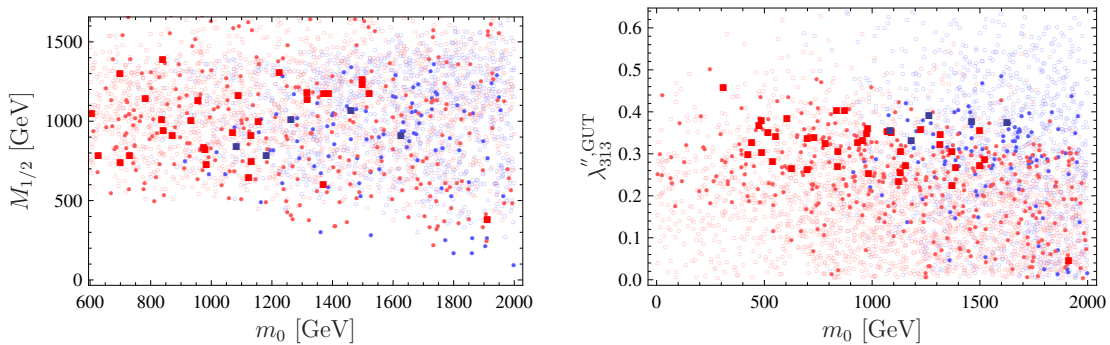


Figure 9. The mass of the lightest stop in the $(m_0, M_{1/2})$ plane (left) and $(m_0, \lambda_{313}^{'',GUT})$ plane (right). Here, we required $m_h \in [122, 130]$ GeV. The blue points have a stable EW vacuum while for the red points deeper CCB vacua exist. The mass of the light stop is indicated by the plot marker: $m_{\tilde{t}_1} < 1$ TeV (open circles), $m_{\tilde{t}_1} < 0.5$ TeV (filled circles), $m_{\tilde{t}_1} < 0.3$ TeV (filled squares).

In Fig. 8 we show the same planes as in Fig. 5, but only for points where the lightest supersymmetric particle (LSP) is the stop. In principle, it is possible to have a stop LSP in the CMSSM without RpV operators [95]. However, these regions are usually very fine-tuned and need very large values of $M_{1/2}$ in order to raise the $\tilde{\chi}_1^0$ mass and to obtain a light Higgs mass in the experimentally preferred range. Therefore, we found no points with a stop LSP and a moderately small RpV coupling $\lambda_{31i}'' < 0.14$ in our scan. In contrast, for larger values of the RpV couplings it is much easier to find a stop LSP. Also here we find that the minimal stop mass is obtained for $\lambda_{31i}'' \simeq 0.3$. We emphasise that the points in Fig. 5, which feature very light stop masses, are exactly the same points as in Fig. 8, which have a stop LSP. This is a non-trivial observation, because $M_{1/2}$ must be large to lift the $\tilde{\chi}_1^0$ mass above the \tilde{t}_1 mass. However, at the same time, a large value of $M_{1/2}$ also raises the \tilde{t}_1 mass via the RGEs.

One might wonder how strong the bias from our parameter choice in Eqs. (4.7) and (4.8) is: It might be possible to find very light stops fulfilling all considered constraints for even larger values of λ_{31i}'' , if the maximal value of m_0 or $M_{1/2}$ is increased. However, this is not the case because this would also increase the size of the radiative corrections to the light stop, as the squarks of the first and second generation also get heavier. To demonstrate that our points with very light stops are not on the edge of our parameter range, we show the correlation between the mass of the light stop and m_0 , $M_{1/2}$ and λ_{31i}'' , respectively, in Fig. 9. The red and blue filled squares denote a stop mass $m_{\tilde{t}_1} < 0.3$ TeV. These are not clustered at the edge of our allowed ranges. In fact, in the R -parity violating coupling the low-mass stops are clustered around $\lambda_{313}'' \sim 0.3$.

We conclude with a brief comment on the collider aspects of the presented scenario. To this affect, we have selected four benchmark points (BP313A, BP313B, BP312A, BP312B) which show the main characteristics of the mass spectra in our preferred parameter regions with very light stops. We give in Table 1 only the most important values but list the entire spectrum and input values in Appendix A.

	BP313A	BP313B	BP312A	BP312B
m_{h_1} [GeV]	124.5	122.3	124.4	122.9
$m_{\tilde{t}_1}$ [GeV]	325.8	247.9	364.6	222.9
$m_{\tilde{t}_2}$ [GeV]	2473.3	1670.9	2227.0	1719.6
$m_{\tilde{b}_1}$ [GeV]	2015.1	1353.5	2215.7	1703.7
$m_{\tilde{d}_R}$ [GeV]	2075.4	1420.8	1896.0	1437.3
$m_{\tilde{s}_R}$ [GeV]	2792.8	1908.1	1896.0	1437.3
$m_{\tilde{q}}$ [GeV]	> 2800	> 1900	> 2500	> 1950
$m_{\tilde{\tau}_1}$ [GeV]	1441.1	1139.3	1446.7	976.1
$m_{\tilde{\chi}_1^0}$ [GeV]	568.2	334.9	480.5	373.3
$m_{\tilde{\chi}_1^+}$ [GeV]	1073.2	639.1	911.3	710.6
$m_{\tilde{g}}$ [GeV]	2834.9	1794.0	2461.0	1955.9

Table 1. Main features of our benchmark points. The full information is given in Appendix A. The benchmarks BP313 have $\lambda''_{313} \neq 0$, while the benchmarks BP312 have $\lambda''_{312} \neq 0$. $m_{\tilde{q}}$ refers to all not explicitly listed squark masses. \tilde{t}_1 is the LSP.

In Table 1, we have summarised all squark masses not given explicitly by $m_{\tilde{q}}$. While the stop mass can be reduced due to the large RpV couplings, all other SUSY scalars are heavy and typically in the multi-TeV range. Also, the gluino is very heavy, and just the electroweakinos can have masses below 1 TeV. Thus for these benchmarks \tilde{t}_1 is the LSP. This mass hierarchy together with the large RpV couplings, yields prompt di-jet decays of the stop LSP, and makes it difficult to look for the light stops at the LHC [32, 94, 96–103]. Therefore, we leave the exploration of possible search strategies for such light stops together with large RpV couplings for future studies.

5 Conclusion

We have discussed the possibility of light stops in a constrained version of the MSSM extended by large R -parity violating couplings λ''_{31i} , $i = 2, 3$. It has been shown that in this model it is possible to find parameter regions providing light stops with masses as low as 250 GeV which are consistent with the Higgs mass measurement, flavour observables and the stability of the electroweak vacuum. This is different from the CMSSM without $\bar{U}D\bar{D}$ operators where large stop mixing or heavy stops are needed to accommodate the Higgs mass. There the presence of light stops is highly constrained by the stability of the electroweak vacuum. Thus stop masses below 800 GeV can hardly be obtained in the R -parity conserving CMSSM. In the CMSSM with large R -parity violation, an interesting observation is that the lightest stop mass is usually found for $\lambda''_{31i} \simeq 0.3$. In these scenarios the lightest stop is usually the LSP. We have shown that for this size of RpV couplings it is necessary to calculate the additional RpV one-loop corrections to the stop mass. These corrections can alter the prediction of the light stop mass by more than 100 GeV compared to an incomplete one-loop calculation that takes into account only R -parity conserving

interactions.

Acknowledgements

We thank Ben Allanach for his fast replies to our questions regarding **SoftSUSY** and Ben O’Leary for many interesting discussions about vacuum stability. NC is supported by the Alexander von Humboldt foundation. HD, FS and TS are supported by the BMBF PT DESY Verbundprojekt 05H2013-THEORIE ‘Vergleich von LHC-Daten mit supersymmetrischen Modellen’.

A Benchmark points

In Tab. 2 we list the explicit parameters, the full sparticle mass spectrum and the predictions for the relevant flavour observables of our four benchmark scenarios. The R_pV coupling is evaluated at the GUT scale and is about 0.3. This results in the lowest possible stop masses in our scan. The sparticle masses are all above 1 TeV, except those of the lightest neutralino $\tilde{\chi}_1^0$ and the lightest stop \tilde{t}_1 . The latter is the LSP for all four benchmark points. Thus we expect the dominant stop decay to be to two jets: $\tilde{t} \rightarrow dd_i$, with possibly a b -jet for $i = 3$.

	BP313A	BP313B	BP312A	BP312B
m_0 [GeV]	1437.8	1182.0	1466.8	1075.7
$M_{1/2}$ [GeV]	1299.1	780.5	1104.4	867.6
$\tan \beta$	12.8	17.2	14.4	22.1
$\text{sign}(\mu)$	+	+	+	+
A_0 [GeV]	-3555.5	-2152.8	-2972.3	-2347.6
$\lambda_{313}^{\prime\prime, \text{GUT}}$	0.310	0.329	0	0
$\lambda_{312}^{\prime\prime, \text{GUT}}$	0	0	0.317	0.335
m_{h_1} [GeV]	124.5	122.3	124.4	122.9
m_{h_2} [GeV]	2523.7	1655.1	2238.6	1571.6
m_A [GeV]	2554.0	1668.4	2253.1	1613.3
m_{H^+} [GeV]	2523.7	1656.3	2238.9	1573.4
$m_{\tilde{t}_1}$ [GeV]	325.8	247.9	364.6	222.9
$m_{\tilde{t}_2}$ [GeV]	2473.3	1670.9	2227.0	1719.6
$m_{\tilde{b}_1}$ [GeV]	2015.1	1353.5	2215.7	1703.7
$m_{\tilde{b}_2}$ [GeV]	2463.7	1658.4	2469.4	1867.8
$m_{\tilde{d}_L}$ [GeV]	2892.5	1961.3	2609.9	2038.0
$m_{\tilde{d}_R}$ [GeV]	2075.4	1420.8	1896.0	1437.3
$m_{\tilde{u}_L}$ [GeV]	2891.6	1959.9	2608.9	2036.7
$m_{\tilde{u}_R}$ [GeV]	2803.8	1914.1	2539.2	1981.3
$m_{\tilde{s}_R}$ [GeV]	2792.8	1908.1	1896.0	1437.3
$m_{\tilde{\tau}_1}$ [GeV]	1441.1	1139.3	1446.7	976.1
$m_{\tilde{\tau}_2}$ [GeV]	1640.5	1256.7	1603.6	1159.7
$m_{\tilde{l}_R}$ [GeV]	1512.7	1215.0	1519.8	1120.1
$m_{\tilde{l}_L}$ [GeV]	1670.4	1288.0	1634.7	1218.2
$m_{\tilde{\chi}_1^0}$ [GeV]	568.2	334.9	480.5	373.3
$m_{\tilde{\chi}_2^0}$ [GeV]	1073.1	639.0	911.2	710.5
$m_{\tilde{\chi}_3^0}$ [GeV]	2019.9	1227.1	1702.0	1334.3
$m_{\tilde{\chi}_4^0}$ [GeV]	2023.1	1231.8	1705.6	1338.6
$m_{\tilde{\chi}_1^+}$ [GeV]	1073.2	639.1	911.3	710.6
$m_{\tilde{\chi}_2^+}$ [GeV]	2023.5	1232.6	1706.2	1339.3
$m_{\tilde{g}}$ [GeV]	2834.9	1794.0	2461.0	1955.9
$R(b \rightarrow s\gamma)$	0.98	0.90	0.96	0.86
$R(B \rightarrow \mu\nu)$	0.99	0.98	0.99	0.98
$R(B_s \rightarrow \mu^+\mu^-)$	1.14	1.18	1.13	1.25
$R(B_d \rightarrow \mu^+\mu^-)$	1.14	1.16	1.13	1.24
$R(\Delta M_{B,s})$	1.01	1.02	1.01	1.02
$R(\Delta M_{B,d})$	1.01	1.02	1.01	1.02
$R(\epsilon_K)$	1.01	1.02	1.02	1.02

Table 2. Full sparticle mass spectrum and flavour observables predicted for our benchmark points. The benchmarks BP313 have $\lambda_{313}^{\prime\prime} \neq 0$, while the benchmarks BP312 have $\lambda_{313}^{\prime\prime} = 0$.

B $\bar{U}\bar{D}\bar{D}$ corrections to stop masses

In the following we give a brief analytical estimate of the one-loop corrections to the stop masses in the presence of large λ'' couplings. The necessary Feynman diagrams are shown in Fig. 10. This also defines our notation for the two-point functions $\Pi^{(\cdot)}$.

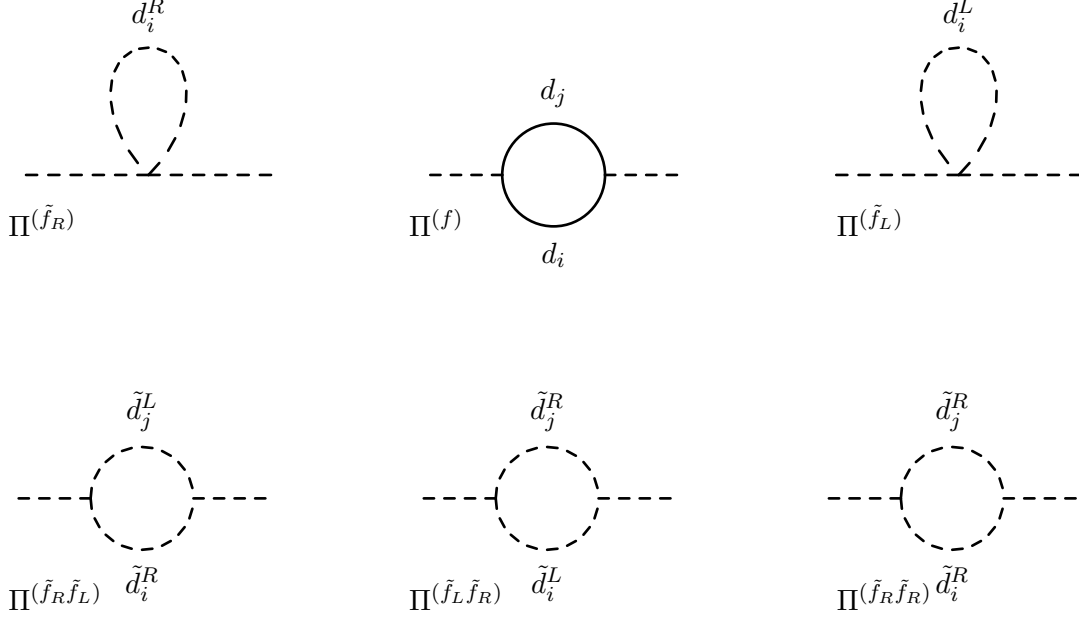


Figure 10. One-loop correction to the stop mass due to down-like (s)quarks.

We start with the corrections which only involve superpotential couplings: since $\Pi^{\tilde{f}L}$ (see Fig. 10) has no contribution from baryon number violating operators, we do not consider it in the following. $\Pi^{\tilde{f}_R\tilde{f}_R}$ only has contributions proportional to the soft-terms T''_λ , which will be discussed below. The amplitudes for the remaining diagrams can be expressed by

$$16\pi^2\Pi^{ff} = (|\Gamma^L(\tilde{t}_R, d_i, d_j)|^2 + |\Gamma^R(\tilde{t}_R, d_i, d_j)|^2)G(p^2, m_{d_i}^2, m_{d_j}^2) \\ - 2(\Gamma^L(\tilde{t}_R, d_i, d_j)\Gamma^R(\tilde{t}_R, d_i, d_j)^* \\ + \Gamma^L(\tilde{t}_R, d_i, d_j)^*\Gamma^R(\tilde{t}_R, d_i, d_j))m_{d_i}m_{d_j}B_0(p^2, m_{d_i}^2, m_{d_j}^2), \quad (\text{B.1})$$

$$16\pi^2\Pi^{\tilde{f}\tilde{f}} = |\Gamma(\tilde{t}_R, \tilde{d}_i^R, \tilde{d}_j^L)|^2 B_0(p^2, m_{\tilde{d}_i^R}^2, m_{\tilde{d}_j^L}^2) + (i \leftrightarrow j), \quad (\text{B.2})$$

$$16\pi^2\Pi^{\tilde{f}} = -\Gamma(\tilde{t}_R, \tilde{t}_R, \tilde{d}_i^R, \tilde{d}_i^R)A_0(m_{\tilde{d}_i^R}^2) + (i \leftrightarrow j). \quad (\text{B.3})$$

with $\Pi^{\tilde{f}\tilde{f}} \equiv \Pi^{\tilde{f}L\tilde{f}R} + \Pi^{\tilde{f}R\tilde{f}L}$. Here, we have introduced

$$G(p^2, m_1^2, m_2^2) \equiv -A_0(m_1^2) - A_0(m_2^2) + (p^2 - m_1^2 - m_2^2)B_0(p^2, m_1^2, m_2^2). \quad (\text{B.4})$$

A_0 and B_0 are the standard Passarino-Veltman integrals [104]. The Γ 's represent the involved vertices. These are given in the limit of diagonal Yukawa couplings by:

1. (Chiral) stop–quark–quark vertex:

$$\begin{aligned}\Gamma^L(\tilde{t}_R, d_i, d_j) &\equiv \lambda''_{3ij}, \\ \Gamma^R(\tilde{t}_R, d_i, d_j) &= 0.\end{aligned}$$

2. Stop–squark–squark vertex:

$$\Gamma(\tilde{t}_R, \tilde{d}_i^R, \tilde{d}_j^L) \equiv \lambda''_{3ij} Y_d^{jj} \langle H_d \rangle = m_{d_j} \lambda''_{3ij}. \quad (\text{B.5})$$

3. Four squark vertex:

$$\Gamma(\tilde{t}_R, \tilde{t}_R, \tilde{d}_i^R, \tilde{d}_j^R) \equiv -\lambda''_{3ik} \lambda''_{3jk}. \quad (\text{B.6})$$

One can check easily that in the limit of unbroken SUSY, $m_{\tilde{d}_i^R} = m_{\tilde{d}_i^L} = m_{d_i}$, the sum of all diagrams vanishes exactly

$$\Pi^{ff} + \Pi^{\tilde{f}\tilde{f}} + \Pi^{\tilde{f}} = 0. \quad (\text{B.7})$$

If we assume for simplicity that all SUSY masses are degenerate ($m_{\tilde{d}_i^R} = m_{\tilde{d}_i^L} = M_{SUSY}$, $\forall i$) and take the limit $p^2 \rightarrow 0$, $M_{SUSY} \gg m_{d_i}$ we obtain a very simple expression for the sum of all diagrams

$$\Pi^{ff} + \Pi^{\tilde{f}\tilde{f}} + \Pi^{\tilde{f}} = \frac{1}{8\pi^2} |\lambda''_{3ij}|^2 M_{SUSY}^2 \equiv \Pi^{\lambda''}. \quad (\text{B.8})$$

Here, we have used

$$B_0(0, m^2, m^2) = \frac{A_0(m^2)}{m^2} - 1, \quad (\text{B.9})$$

$$A_0(m^2) = m^2 - m^2 \log \frac{m^2}{Q^2}, \quad (\text{B.10})$$

and set as the renormalisation scale $Q = M_{SUSY}$.

As mentioned above there is also another one–loop contribution due to the trilinear soft-breaking terms:

$$16\pi^2 \Pi^{\tilde{f}_R \tilde{f}_R} = |T''_{3ij}|^2 B_0(p^2, m_{\tilde{d}_i^R}^2, m_{\tilde{d}_j^R}^2). \quad (\text{B.11})$$

However, this contribution vanishes exactly in the limit of degenerate down–like squark masses $m_{\tilde{d}_i^R} = m_{\tilde{d}_j^R} = Q = M_{SUSY}$. Hence, it can only play a role in the case of a large mass splitting between the squarks in the loop. To see this, we can use $m_{\tilde{d}_i^R} = Q = M_{SUSY}$ together with $m_{\tilde{d}_j^R} = M_{SUSY} + \delta$ and obtain

$$\Pi^{\tilde{f}_R \tilde{f}_R} = -\frac{\delta^2}{16\pi^2 M_{SUSY}^2} |T''_{3ij}|^2. \quad (\text{B.12})$$

Here, we have made use of

$$B_0(0, m_1^2, m_2^2) = -\log \frac{m_2^2}{Q^2} + \frac{1}{m_2^2 - m_1^2} \left(m_2^2 - m_1^2 + m_1^2 \log \frac{m_1^2}{m_2^2} \right). \quad (\text{B.13})$$

We can now use the derived expressions for the one-loop self-energies to calculate the stop mass at one-loop. If we neglect flavour mixing in the squark sector, the one-loop stop masses are the eigenvalues of the one-loop corrected stop mass matrix $m_t^{2,(1L)}$ given by

$$m_t^{2,(1L)} = m_t^{2,T} + \delta m^{2,MSSM} + (\Pi^{\lambda''} + \Pi^{\tilde{f}_R \tilde{f}_R}) \begin{pmatrix} 0 & 0 \\ 0 & 1 \end{pmatrix}. \quad (\text{B.14})$$

Here, $m_t^{2,T}$ is the stop mass matrix at tree-level,

$$m_t^{2,T} = \begin{pmatrix} m_{\tilde{t}_L}^2 - \frac{1}{24}(g_1^2 - 3g_2^2)(v_d^2 - v_u^2) + \frac{v_u^2}{2}|Y_t|^2 & \frac{1}{\sqrt{2}}(v_u T_t^* - v_d \mu Y_t^*) \\ \frac{1}{\sqrt{2}}(v_u T_t - v_d Y_t \mu^*) & m_{\tilde{t}_R}^2 + \frac{v_u^2}{2}|Y_t|^2 + \frac{1}{6}g_1^2(v_d^2 - v_u^2) \end{pmatrix}, \quad (\text{B.15})$$

and $\delta m^{2,MSSM}$ is the matrix for the well known corrections which do not involve R -parity violating couplings, see e.g. Ref. [105].

C Minimising the scalar potential of the MSSM with $\bar{U}\bar{D}\bar{D}$ operators

We discuss in the following the scalar potential in the MSSM in the presence of λ_{3ij}'' couplings and vevs for stops, staus, as well as the down-type squarks at tree-level. The checks performed by `Vevacious` include also the one-loop corrections to the effective potential. However, these expressions are not shown here because of their length. To simplify the expressions we assume here that the Yukawa couplings and the soft-breaking parameters in the R -parity conserving sector are diagonal:

$$\begin{aligned} Y_\tau &= Y_{e,33}, & Y_b &= Y_{d,33}, & Y_t &= Y_{u,33}, \\ T_\tau &= T_{e,33}, & T_b &= T_{d,33}, & T_t &= T_{u,33}, \\ m_{\tilde{t}_L}^2 &= m_{\tilde{Q},33}^2, & m_{\tilde{t}_R}^2 &= m_{\tilde{U},33}^2, \\ m_{\tilde{\tau}_L}^2 &= m_{\tilde{L},33}^2, & m_{\tilde{\tau}_R}^2 &= m_{\tilde{E},33}^2, \\ m_{\tilde{q}_i}^2 &= m_{\tilde{Q},ii}^2, & m_{\tilde{d}_i}^2 &= m_{\tilde{D},33}^2. \end{aligned}$$

The full expression in the limit of diagonal Yukawa and R -parity conserving soft terms read

$$\begin{aligned} V_{H_d, H_u}^{\text{tree}} &= \frac{1}{32} (g_1^2(v_d^2 - v_u^2)^2 + g_2^2(v_d^2 - v_u^2)^2) \\ &\quad - B_\mu v_d v_u + \frac{1}{2} (|\mu|^2(v_d^2 + v_u^2) + m_{H_d}^2 v_d^2 + m_{H_u}^2 v_u^2), \end{aligned} \quad (\text{C.1})$$

$$\begin{aligned} V_{H_d, H_u, \tilde{\tau}_L, \tilde{\tau}_R}^{\text{tree}} &= \frac{1}{32} (g_1^2(v_{\tau_L}^2 - 2v_{\tau_R}^2)^2 + g_2^2(v_{\tau_L}^2)^2) \\ &\quad + \frac{1}{4} (Y_\tau^2(v_d^2 v_{\tau_L}^2 + v_d^2 v_{\tau_R}^2 + v_{\tau_L}^2 v_{\tau_R}^2) + \frac{1}{\sqrt{2}} v_{\tau_L} v_{\tau_R} (T_\tau v_d - Y_\tau \mu v_u)) \\ &\quad + \frac{1}{2} (m_{\tilde{\tau}_L}^2 v_{\tau_L}^2 + m_{\tilde{\tau}_R}^2 v_{\tau_R}^2), \end{aligned} \quad (\text{C.2})$$

$$\begin{aligned}
V_{H_d, H_u, \tilde{t}_L, \tilde{t}_R}^{\text{tree}} = & \frac{1}{288} \left[3 \left(4(6(v_{\tilde{t}_L}^2 (2m_{\tilde{t}_L}^2 + Y_t^2(v_{\tilde{t}_R}^2 + v_u^2)) + v_{\tilde{t}_R}^2 (2m_{\tilde{t}_R}^2 + v_u^2 Y_t^2) \right. \right. \\
& + 2\sqrt{2}v_{\tilde{t}_L}v_{\tilde{t}_R}(v_u T_t - v_d Y_t \mu) + g_3^2(v_{\tilde{t}_L}^2 - v_{\tilde{t}_R}^2)^2 + \\
& 3g_2^2(-2v_u^2 v_{\tilde{t}_L}^2 + 2v_d^2 v_{\tilde{t}_L}^2 + v_{\tilde{t}_L}^4) + g_1^2((v_{\tilde{t}_L}^2 - 4v_{\tilde{t}_R}^2)(v_{\tilde{t}_L}^2 - 4v_{\tilde{t}_R}^2 + 6v_u^2) \\
& \left. \left. - 6v_d^2(v_{\tilde{t}_L}^2 - 4v_{\tilde{t}_R}^2)) \right) \right], \tag{C.3}
\end{aligned}$$

$$\begin{aligned}
V_{H_d, H_u, \tilde{d}_L^i, \tilde{d}_R^i}^{\text{tree}} = & \frac{1}{288} \left[3 \left(4(6(v_{D_R^i}^2 (2m_{\tilde{d}_i}^2 + Y_{d_i}^2(v_{D_L^i}^2 + v_d^2)) + v_{D_L^i}^2 (2m_{\tilde{q}_i}^2 + v_d^2 Y_{d_i}^2) \right. \right. \\
& + 2\sqrt{2}v_{D_L^i}v_{D_R^i}(v_d T_{d_i} - v_u Y_{d_i} \mu) + g_3^2(v_{D_L^i}^2 - v_{D_R^i}^2)^2) \\
& + 3g_2^2(v_{D_L^i}^4 + 2v_{D_L^i}^2(v_u^2 - v_d^2)) + g_1^2(6v_u^2(v_{D_L^i}^2 + 2v_{D_R^i}^2) \\
& \left. \left. + (v_{D_L^i}^2 + 2v_{D_R^i}^2)(v_{D_L^i}^2 - 6v_d^2 + 2v_{D_R^i}^2)) \right) \right], \tag{C.4}
\end{aligned}$$

$$V_{H_d, H_u, \tilde{d}_L^j, \tilde{d}_R^j}^{\text{tree}} = V_{H_d, H_u, \tilde{d}_L^i, \tilde{d}_R^i}^{\text{tree}} \mid (i \rightarrow j), \tag{C.5}$$

$$\begin{aligned}
V_{\tilde{t}_L, \tilde{t}_R, \tilde{d}_L^i, \tilde{d}_R^i}^{\text{tree}} = & \frac{1}{144} \left[g_1^2(v_{D_L^i}^2 + 2v_{D_R^i}^2)(v_{\tilde{t}_L}^2 - 4v_{\tilde{t}_R}^2) - 9g_2^2 v_{D_L^i}^2 v_{\tilde{t}_L}^2 \right. \\
& \left. - 6g_3^2(v_{D_L^i}^2 - v_{D_R^i}^2)(v_{\tilde{t}_L}^2 - v_{\tilde{t}_R}^2) \right], \tag{C.6}
\end{aligned}$$

$$V_{\tilde{t}_L, \tilde{t}_R, \tilde{d}_L^j, \tilde{d}_R^j}^{\text{tree}} = V_{\tilde{t}_L, \tilde{t}_R, \tilde{d}_L^i, \tilde{d}_R^i}^{\text{tree}} \mid (i \rightarrow j), \tag{C.7}$$

$$\begin{aligned}
V_{\tilde{d}_L^i, \tilde{d}_R^i, \tilde{d}_L^j, \tilde{d}_R^j}^{\text{tree}} = & \frac{1}{144} \left[g_1^2(v_{D_L^i}^2 + 2v_{D_R^i}^2)(v_{D_L^j}^2 + 2v_{D_R^j}^2) + 9g_2^2 v_{D_L^i}^2 v_{D_L^j}^2 \right. \\
& \left. - 6g_3^2(v_{D_L^j}^2 - v_{D_R^j}^2)(v_{D_L^i}^2 - v_{D_R^i}^2) + 72v_{D_L^j}v_{D_R^j}v_{D_L^i}v_{D_R^i}Y_{d_i}Y_{d_j} \right], \tag{C.8}
\end{aligned}$$

$$\begin{aligned}
V_{\tilde{t}_R, \tilde{t}_R, \tilde{d}_R^i, \tilde{d}_R^j}^{\text{tree}} = & \frac{1}{4} \left[\lambda_{3ij}^{\prime\prime, 2} (v_{D_R^j}^2 (v_{D_R^i}^2 + v_{\tilde{t}_R}^2) + v_{D_R^i}^2 v_{\tilde{t}_R}^2) \right. \\
& - 2\lambda_{3ij}^{\prime\prime} (v_{D_L^j}v_d v_{D_R^i}v_{\tilde{t}_R}Y_{d_j} + v_{D_R^j}v_{D_L^i}v_d v_{\tilde{t}_R}Y_{d_i} + v_{D_R^j}v_{D_R^i}v_{\tilde{t}_L}v_u Y_t) \\
& \left. - 2\sqrt{2}T_{\lambda_{3ij}^{\prime\prime}} v_{D_R^j}v_{D_R^i}v_{\tilde{t}_R} \right]. \tag{C.9}
\end{aligned}$$

The D -term contributions are minimised for

$$v_{D_L^i} = v_{D_R^i}, \quad v_{D_L^j} = v_{D_R^j}, \quad v_{\tilde{t}_L} = v_{\tilde{t}_R}, \quad v_u = v_d. \tag{C.10}$$

In addition, for $j = 3$ we neglect the terms involving Y_{d_i} and T_{d_i} which correspond to first or second generation Yukawas, respectively, trilinear terms. In this limit all terms involving down-squark vevs read

$$\begin{aligned}
V_{v_{D_R^i}, v_{D_R^j}}^{\text{tree}} = & v_{D_R^i}^2 \left(\frac{1}{2}(m_{\tilde{d}_i}^2 + m_{\tilde{q}_i}^2) + \frac{\lambda_{3ij}^{\prime\prime, 2} v_{\tilde{t}_R}^2}{4} \right) \\
& + v_{D_R^j}^2 \left(\frac{1}{2}(m_{\tilde{d}_j}^2 + m_{\tilde{q}_j}^2) + \frac{v_d T_{d_j}}{\sqrt{2}} + \frac{\lambda_{3ij}^{\prime\prime, 2} v_{\tilde{t}_R}^2}{4} + \frac{1}{2}v_d^2 Y_{d_j}^2 - \frac{v_d Y_{d_j} \mu}{\sqrt{2}} + \frac{v_{D_R^j}^2 Y_{d_j}^2}{4} \right) \\
& + \frac{v_{D_R^j} v_{D_R^i}}{4} \left(\lambda_{3ij}^{\prime\prime, 2} v_{D_R^j} v_{D_R^i} - 2\lambda_{3ij}^{\prime\prime} v_d v_{\tilde{t}_R} (Y_{d_j} + Y_t) - 2\sqrt{2}T_{\lambda_{3ij}^{\prime\prime}} v_{\tilde{t}_R} \right) \\
& + \frac{g_1^2 + g_2^2}{32} \left((v_{D_R^j}^2 + v_{D_R^i}^2) (v_{D_R^j}^2 + v_{D_R^i}^2 - 2v_{\tilde{t}_R}^2) \right). \tag{C.11}
\end{aligned}$$

The first line on the right hand side is always positive. Especially since the β -function of $m_{\tilde{q}_i}^2$ has no terms proportional to λ'' or to a third generation Yukawa coupling at one-loop it is positive and usually much larger than the other soft-parameter involved. This makes it rather unlikely that $v_{D_R^i} \neq 0$ are preferred at the minimum of the potential. However, in the limit $v_{D_R^i} \rightarrow 0$ the entire first and third line vanish. The form of the potential then has a similar form to the potential when considering only stop and Higgs vevs. However, usually $m_{\tilde{q}_i}^2 > m_{\tilde{t}_L}^2$ and $m_{\tilde{d}_i}^2 > m_{\tilde{t}_R}^2$ holds. This makes it unlikely that the down-squarks gain a vev before the stops do. Thus, one can expect that the check for the additional down-squark vevs put only weak constraints in addition for points with very large $\tan \beta$. While the discussion has been so far rather hand-waving the general statement has been confirmed in our numerical studies: Only 5% of the points with stop masses below 1 TeV which pass the stability check including only stop vevs fail the additional test that includes sbottom vevs. Including sdown and sstrange vevs does not put any additional constraint. For comparison: About 1/3 of the entire points in the scan fail the check for a stable vacuum when checking for stop and stau vevs. In the interesting parameter range of stop masses below 1 TeV even 2/3 are ruled out.

References

- [1] S. P. Martin [hep-ph/9709356](#).
- [2] H. P. Nilles Phys.Rept. **110** (1984) 1–162.
- [3] P. Bechtle, K. Desch, H. K. Dreiner, M. Hamer, M. Krämer, *et. al.* [arXiv:1310.3045](#).
- [4] N. Craig [arXiv:1309.0528](#).
- [5] P. Bechtle, T. Bringmann, K. Desch, H. Dreiner, M. Hamer, *et. al.* JHEP **1206** (2012) 098, [[arXiv:1204.4199](#)].
- [6] O. Buchmueller, R. Cavanaugh, M. Citron, A. De Roeck, M. Dolan, *et. al.* Eur.Phys.J. **C72** (2012) 2243, [[arXiv:1207.7315](#)].
- [7] ATLAS Collaboration, G. Aad *et. al.* Phys.Lett. **B716** (2012) 1–29, [[arXiv:1207.7214](#)].
- [8] CMS Collaboration, S. Chatrchyan *et. al.* Phys.Lett. **B716** (2012) 30–61, [[arXiv:1207.7235](#)].
- [9] M. S. Carena, H. Haber, S. Heinemeyer, W. Hollik, C. Wagner, *et. al.* Nucl.Phys. **B580** (2000) 29–57, [[hep-ph/0001002](#)].
- [10] S. Heinemeyer, W. Hollik, and G. Weiglein Eur.Phys.J. **C9** (1999) 343–366, [[hep-ph/9812472](#)].
- [11] J. Camargo-Molina, B. O’Leary, W. Porod, and F. Staub [arXiv:1309.7212](#).
- [12] N. Blinov and D. E. Morrissey [arXiv:1310.4174](#).
- [13] D. Chowdhury, R. M. Godbole, K. A. Mohan, and S. K. Vempati [arXiv:1310.1932](#).
- [14] J. Camargo-Molina, B. Garbrecht, B. O’Leary, W. Porod, and F. Staub [arXiv:1405.7376](#).
- [15] A. Birkedal, Z. Chacko, and M. K. Gaillard JHEP **0410** (2004) 036, [[hep-ph/0404197](#)].
- [16] S. Chang, P. J. Fox, and N. Weiner JHEP **0608** (2006) 068, [[hep-ph/0511250](#)].

- [17] L. J. Hall, D. Pinner, and J. T. Ruderman *JHEP* **1204** (2012) 131, [[arXiv:1112.2703](#)].
- [18] A. Delgado, C. Kolda, and A. de la Puente *Phys.Lett.* **B710** (2012) 460–466, [[arXiv:1111.4008](#)].
- [19] M. Perelstein and B. Shakya *Phys.Rev.* **D88** (2013), no. 7 075003, [[arXiv:1208.0833](#)].
- [20] A. Kaminska, G. G. Ross, and K. Schmidt-Hoberg [arXiv:1308.4168](#).
- [21] G. G. Ross, K. Schmidt-Hoberg, and F. Staub *JHEP* **1208** (2012) 074, [[arXiv:1205.1509](#)].
- [22] G. G. Ross and K. Schmidt-Hoberg *Nucl.Phys.* **B862** (2012) 710–719, [[arXiv:1108.1284](#)].
- [23] X. Lu, H. Murayama, J. T. Ruderman, and K. Tobioka [arXiv:1308.0792](#).
- [24] A. Kaminska, G. G. Ross, K. Schmidt-Hoberg, and F. Staub [arXiv:1401.1816](#).
- [25] L. J. Hall and M. Suzuki *Nucl.Phys.* **B231** (1984) 419.
- [26] R. Barbier, C. Berat, M. Besancon, M. Chemtob, A. Deandrea, et. al. *Phys.Rept.* **420** (2005) 1–202, [[hep-ph/0406039](#)].
- [27] H. K. Dreiner [hep-ph/9707435](#).
- [28] B. Allanach, A. Dedes, and H. Dreiner *Phys.Rev.* **D69** (2004) 115002, [[hep-ph/0309196](#)].
- [29] B. Allanach and B. Gripaios *JHEP* **1205** (2012) 062, [[arXiv:1202.6616](#)].
- [30] M. Asano, K. Rolbiecki, and K. Sakurai *JHEP* **1301** (2013) 128, [[arXiv:1209.5778](#)].
- [31] R. Franceschini and R. Torre *Eur.Phys.J.* **C73** (2013) 2422, [[arXiv:1212.3622](#)].
- [32] J. A. Evans and Y. Kats *JHEP* **1304** (2013) 028, [[arXiv:1209.0764](#)].
- [33] H. K. Dreiner and G. G. Ross *Nucl.Phys.* **B365** (1991) 597–613.
- [34] H. Dreiner, S. Grab, and T. Stefaniak *Phys.Rev.* **D84** (2011) 035023, [[arXiv:1102.3189](#)].
- [35] H. Dreiner and T. Stefaniak *Phys.Rev.* **D86** (2012) 055010, [[arXiv:1201.5014](#)].
- [36] H. Dreiner, F. Staub, A. Vicente, and W. Porod *Phys.Rev.* **D86** (2012) 035021, [[arXiv:1205.0557](#)].
- [37] G. R. Farrar and P. Fayet *Phys.Lett.* **B76** (1978) 575–579.
- [38] S. Weinberg *Phys.Rev.* **D26** (1982) 287.
- [39] N. Sakai and T. Yanagida *Nucl.Phys.* **B197** (1982) 533.
- [40] A. H. Chamseddine and H. K. Dreiner *Nucl.Phys.* **B458** (1996) 65–89, [[hep-ph/9504337](#)].
- [41] H. M. Lee, S. Raby, M. Ratz, G. G. Ross, R. Schieren, et. al. *Nucl.Phys.* **B850** (2011) 1–30, [[arXiv:1102.3595](#)].
- [42] H. K. Dreiner, M. Hanussek, and C. Luhn *Phys.Rev.* **D86** (2012) 055012, [[arXiv:1206.6305](#)].
- [43] J. E. Kim and H. P. Nilles *Phys.Lett.* **B138** (1984) 150.
- [44] G. Giudice and A. Masiero *Phys.Lett.* **B206** (1988) 480–484.
- [45] J. Goity and M. Sher *Phys.Lett.* **B346** (1995) 69–74, [[hep-ph/9412208](#)].
- [46] B. Allanach, A. Dedes, and H. K. Dreiner *Phys.Rev.* **D60** (1999) 075014, [[hep-ph/9906209](#)].
- [47] H. Dreiner, K. Nickel, and F. Staub [arXiv:1309.1735](#).
- [48] H. P. Nilles, M. Srednicki, and D. Wyler *Phys.Lett.* **B120** (1983) 346.

- [49] H. E. Haber Nucl.Phys.Proc.Suppl. **62** (1998) 469–484, [[hep-ph/9709450](#)].
- [50] H. E. Haber and R. Hempfling Phys.Rev. **D48** (1993) 4280–4309, [[hep-ph/9307201](#)].
- [51] M. S. Carena, M. Quiros, and C. Wagner Nucl.Phys. **B461** (1996) 407–436, [[hep-ph/9508343](#)].
- [52] S. Heinemeyer, W. Hollik, and G. Weiglein Phys.Lett. **B455** (1999) 179–191, [[hep-ph/9903404](#)].
- [53] ATLAS Collaboration, G. Aad et. al. [arXiv:1407.0603](#).
- [54] B. Allanach, A. Dedes, and H. K. Dreiner Phys.Rev. **D60** (1999) 056002, [[hep-ph/9902251](#)].
- [55] F. Staub Comput.Phys.Comm. **182** (2011) 808–833, [[arXiv:1002.0840](#)].
- [56] F. Staub, W. Porod, and B. Herrmann JHEP **1010** (2010) 040, [[arXiv:1007.4049](#)].
- [57] A. Donini Nucl.Phys. **B467** (1996) 3–24, [[hep-ph/9511289](#)].
- [58] F. Staub [arXiv:0806.0538](#).
- [59] F. Staub Comput.Phys.Comm. **181** (2010) 1077–1086, [[arXiv:0909.2863](#)].
- [60] F. Staub Computer Physics Communications **184** (2013) pp. 1792–1809, [[arXiv:1207.0906](#)].
- [61] F. Staub [arXiv:1309.7223](#).
- [62] W. Porod Comput.Phys.Comm. **153** (2003) 275–315, [[hep-ph/0301101](#)].
- [63] W. Porod and F. Staub Comput.Phys.Comm. **183** (2012) 2458–2469, [[arXiv:1104.1573](#)].
- [64] A. Brignole, G. Degrandi, P. Slavich, and F. Zwirner Nucl.Phys. **B631** (2002) 195–218, [[hep-ph/0112177](#)].
- [65] A. Brignole, G. Degrandi, P. Slavich, and F. Zwirner Nucl.Phys. **B643** (2002) 79–92, [[hep-ph/0206101](#)].
- [66] A. Dedes and P. Slavich Nucl.Phys. **B657** (2003) 333–354, [[hep-ph/0212132](#)].
- [67] A. Dedes, G. Degrandi, and P. Slavich Nucl.Phys. **B672** (2003) 144–162, [[hep-ph/0305127](#)].
- [68] B. Allanach Comput.Phys.Comm. **143** (2002) 305–331, [[hep-ph/0104145](#)].
- [69] B. Allanach and M. Bernhardt Comput.Phys.Comm. **181** (2010) 232–245, [[arXiv:0903.1805](#)].
- [70] B. Allanach, S. Kraml, and W. Porod JHEP **0303** (2003) 016, [[hep-ph/0302102](#)].
- [71] P. Bechtle, O. Brein, S. Heinemeyer, G. Weiglein, and K. E. Williams Comput.Phys.Comm. **181** (2010) 138–167, [[arXiv:0811.4169](#)].
- [72] P. Bechtle, O. Brein, S. Heinemeyer, G. Weiglein, and K. E. Williams Comput.Phys.Comm. **182** (2011) 2605–2631, [[arXiv:1102.1898](#)].
- [73] P. Bechtle, O. Brein, S. Heinemeyer, O. Stal, T. Stefaniak, et. al. PoS CHARGED2012 (2012) 024, [[arXiv:1301.2345](#)].
- [74] P. Bechtle, O. Brein, S. Heinemeyer, O. Stal, T. Stefaniak, et. al. Eur.Phys.J. **C74** (2014) 2693, [[arXiv:1311.0055](#)].
- [75] P. Bechtle, S. Heinemeyer, O. Stål, T. Stefaniak, and G. Weiglein Eur.Phys.J. **C74** (2014) 2711, [[arXiv:1305.1933](#)].

- [76] P. Bechtle, S. Heinemeyer, O. Stål, T. Stefaniak, and G. Weiglein [arXiv:1403.1582](#).
- [77] A. Belyaev, S. Khalil, S. Moretti, and M. C. Thomas JHEP **1405** (2014) 076, [[arXiv:1312.1935](#)].
- [78] W. Porod, F. Staub, and A. Vicente [arXiv:1405.1434](#).
- [79] H. Dreiner, K. Nickel, W. Porod, and F. Staub Comput.Phys.Commun. **184** (2013) 2604–2617, [[arXiv:1212.5074](#)].
- [80] Particle Data Group, J. Beringer *et. al.* Phys.Rev. **D86** (2012) 010001.
- [81] M. Misiak Acta Phys.Polon. **B40** (2009) 2987–2996, [[arXiv:0911.1651](#)].
- [82] Heavy Flavor Averaging Group, D. Asner *et. al.* [arXiv:1010.1589](#).
- [83] Particle Data Group, K. Nakamura *et. al.* J.Phys. **G37** (2010) 075021.
- [84] U. Haisch and F. Mahmoudi JHEP **1301** (2013) 061, [[arXiv:1210.7806](#)].
- [85] CMS Collaboration, S. Chatrchyan *et. al.* Phys.Rev.Lett. **111** (2013) 101804, [[arXiv:1307.5025](#)].
- [86] LHCb collaboration, R. Aaij *et. al.* Phys.Rev.Lett. **111** (2013) 101805, [[arXiv:1307.5024](#)].
- [87] A. J. Buras, M. Jamin, and P. H. Weisz Nucl.Phys. **B347** (1990) 491–536.
- [88] E. Golowich, J. Hewett, S. Pakvasa, A. A. Petrov, and G. K. Yeghiyan Phys.Rev. **D83** (2011) 114017, [[arXiv:1102.0009](#)].
- [89] M. Arana-Catania [arXiv:1312.4888](#).
- [90] J. Camargo-Molina, B. O’Leary, W. Porod, and F. Staub [arXiv:1307.1477](#).
- [91] F. Staub, T. Ohl, W. Porod, and C. Speckner Comput.Phys.Commun. **183** (2012) 2165–2206, [[arXiv:1109.5147](#)].
- [92] ATLAS Collaboration, G. Aad *et. al.* [arXiv:1405.7875](#).
- [93] CMS Collaboration, S. Chatrchyan *et. al.* Phys.Lett. **B718** (2012) 329–347, [[arXiv:1208.2931](#)].
- [94] CMS Collaboration, S. Chatrchyan *et. al.* Phys.Lett. **B730** (2014) 193–214, [[arXiv:1311.1799](#)].
- [95] J. Ellis, K. A. Olive, and J. Zheng [arXiv:1404.5571](#).
- [96] CMS Collaboration, S. Chatrchyan *et. al.* Phys.Rev.Lett. **110** (2013) 141802, [[arXiv:1302.0531](#)].
- [97] CMS Collaboration, S. Chatrchyan *et. al.* Phys.Lett. **B704** (2011) 123–142, [[arXiv:1107.4771](#)].
- [98] CMS Collaboration, S. Chatrchyan *et. al.* Phys.Rev. **D87** (2013), no. 11 114015, [[arXiv:1302.4794](#)].
- [99] ATLAS Collaboration, G. Aad *et. al.* Phys.Lett. **B708** (2012) 37–54, [[arXiv:1108.6311](#)].
- [100] ATLAS Collaboration, G. Aad *et. al.* JHEP **1301** (2013) 029, [[arXiv:1210.1718](#)].
- [101] ATLAS Collaboration. ATLAS-CONF-2012-148, ATLAS-COM-CONF-2012-180.
- [102] D. Duggan, J. A. Evans, J. Hirschauer, K. Kaadze, D. Kolchmeyer, *et. al.* [arXiv:1308.3903](#).
- [103] Y. Bai, A. Katz, and B. Tweedie JHEP **1401** (2014) 040, [[arXiv:1309.6631](#)].

- [104] G. Passarino and M. Veltman Nucl.Phys. **B160** (1979) 151.
- [105] D. M. Pierce, J. A. Bagger, K. T. Matchev, and R.-j. Zhang Nucl.Phys. **B491** (1997) 3–67,
[[hep-ph/9606211](#)].